

Analysis of the anomalous Doppler effect from quantum theory to classical dynamics simulations

Xinhang Xu(徐新航), Jinlin Xie(谢锦林), Jian Liu(刘健), and Wandong Liu(刘万东)
Citation: Chin. Phys. B, 2025, 34 (**12**): 120301. DOI: 10.1088/1674-1056/ade8e4
http://cpb.iphy.ac.cn; http://iopscience.iop.org/cpb

What follows is a list of articles you may be interested in

Multicast-oriented key provision in hybrid DV/CV multi-domain quantum networks

Xinyu Chen(陈欣宇), Yuan Cao(曹原), Yuxiang Lu(陆宇翔), Yue Chen(陈越), Kunpeng Zheng(郑昆朋), Xiaosong Yu(郁小松), Yongli Zhao(赵永利), Jie Zhang(张杰), and Qin Wang(王琴)
Chin. Phys. B, 2025, 34 (**9**): 090301. DOI: 10.1088/1674-1056/adecf8

Witnessing the distribution of sources in quantum networks via hierarchical nonlocality

Shu-Yuan Yang(杨舒媛), Jin-Chuan Hou(侯晋川), and Kan He(贺衍)
Chin. Phys. B, 2025, 34 (**6**): 060303. DOI: 10.1088/1674-1056/add507

Periodic modulation of adiabatic dynamics in non-reciprocal Landau-Zener systems

Rong Chang(常蓉) and Sheng-Chang Li(栗生长)
Chin. Phys. B, 2025, 34 (**3**): 030305. DOI: 10.1088/1674-1056/adab64

Entanglement and energy transportation in central-spin quantum battery

Fan Liu(刘帆), Hui-Yu Yang(杨慧宇), Shuai-Li Wang(王帅立), Jun-Zhong Wang(王俊钟), Kun Zhang(张堃), and Xiao-Hui Wang(王晓辉)
Chin. Phys. B, 2025, 34 (**2**): 020306. DOI: 10.1088/1674-1056/ad9a9d

Single-photon scattering controlled by an imperfect cavity

Liwei Duan(段立伟), Qing-Hu Chen(陈庆虎)
Chin. Phys. B, 2020, 29 (**7**): 070301. DOI: 10.1088/1674-1056/ab90ee

---

Analysis of the anomalous Doppler effect from quantum theory to classical dynamics simulations

Xinhang Xu(徐新航)[1], Jinlin Xie(谢锦林)[1,†], Jian Liu(刘健)[2], and Wandong Liu(刘万东)[1]

[1] *Department of Plasma Physics and Fusion Engineering, University of Science and Technology of China, Hefei* 230026, *China*
[2] *Weihai Institute for Interdisciplinary Research, Shandong University, Weihai* 264209, *China*

(Received 12 May 2025; revised manuscript received 13 June 2025; accepted manuscript online 27 June 2025)

The fundamental physics of anomalous and normal Doppler resonances between electrons and electromagnetic (EM) waves is analyzed using a quantum model that incorporates angular-momentum conservation. This work extends prior theory by explicitly linking the resonant integer m to the EM wave's angular-momentum quantum number. Numerical simulations based on the volume-preserving algorithm (VPA) further confirm this correspondence. Moreover, a direct comparison of the energy-transfer ratio from translational energy to gyrokinetic energy during resonance, between classical dynamics and quantum predictions, is presented and verified numerically.

Keywords: anomalous Doppler effect, resonant condition, angular momentum conservation

PACS: 03.65.−w, 33.35.+r, 02.60.Cb, 12.20.−m

DOI: 10.1088/1674-1056/ade8e4 **CSTR:** 32038.14.CPB.ade8e4

1. Introduction

The anomalous Doppler effect (ADE),[1–4] in which the observed frequency shift behaves contrary to the conventional Doppler effect under specific conditions, was first theoretically predicted by Soviet physicist Ginzburg.[3] This phenomenon arises when a system moves with a velocity exceeding the phase velocity of light in the medium, transferring its translational kinetic energy into internal energy while emitting radiation. A notable example, discussed by Frank in his 1958 Nobel lecture,[2] shows that radiation emission does not occur through the typical transition from an excited state to a lower energy level. Instead, it proceeds from a lower to a higher energy level, powered by the system's translational kinetic energy. This counterintuitive prediction has attracted considerable attention and has inspired extensive research.[5–12]

In 1967, Artsimovich *et al.*[13] reported discrepancies in tokamak experiments: the electron temperature estimated from diamagnetic signals was significantly higher than that derived from electrical-conductivity measurements. Although unrecognized at the time, this anomaly may represent the first experimental observation of ADE. In 1968, Kadomtsev and Pogutse[14] identified ADE as the underlying mechanism, in which electrons undergo velocity scattering from the longitudinal to the transverse direction under resonant conditions. This process enhances the diamagnetic effect beyond what would be expected from thermal motion alone. Subsequently, a range of ADE-related phenomena have been observed, including electron-beam scattering in magnetic-field vacuum tubes,[2] wave radiation,[15–17] and runaway-electron instabilities in tokamaks.[18,19] The ADE has also given rise to practical applications, notably in high-power microwave generation and in mitigating runaway electrons in tokamak fusion reactors.[9,20]

The physics of the ADE was first elucidated through quantum analysis by Frank[2] and Ginzburg.[21] In this work, we extend Ginzburg's quantum framework by incorporating the conservation of angular momentum to provide a more rigorous analysis of ADE. This approach yields new insights into the relationship between wave angular momentum and ADE under resonant conditions, which is referred to as anomalous Doppler resonance (ADR). For an electron moving in a magnetic field and interacting with an external electromagnetic (EM) wave, the general resonance condition is given by

$$\omega = m\omega_{\rm ce} + \boldsymbol{k}\cdot\boldsymbol{v},$$

where $\boldsymbol{k}$ is the wave vector, $\omega_{\rm ce}$ is the electron cyclotron frequency (here $\omega_{\rm ce} > 0$), $\boldsymbol{v}$ is the electron velocity, and ω is the wave angular frequency, while $m = 0, \pm1, \pm2, \ldots$ represents the Landau level.[22] Specifically, for plane EM waves, we find that resonance is restricted to the fundamental harmonics ($m = \pm1$) due to spin angular-momentum conservation, reducing the condition to

$$\omega = \pm\omega_{\rm ce} + \boldsymbol{k}\cdot\boldsymbol{v},$$

where the negative sign refers to the ADR condition, while the positive sign refers to the normal Doppler resonance (NDR) condition. This represents a significant constraint compared to previous theoretical treatments[23] which suggested possible resonance at all harmonic orders ($m = \pm1, \pm2, \ldots$) for plane

†Corresponding author. E-mail: jlxie@ustc.edu.cn

© 2025 Chinese Physical Society and IOP Publishing Ltd. All rights, including for text and data mining, AI training, and similar technologies, are reserved.

EM wave. Despite the simplicity of the model, our analysis demonstrates that angular-momentum conservation plays a crucial role in EM wave–electron resonance — an aspect that, to the best of our knowledge, has not been previously addressed in the literature.

Furthermore, we perform numerical simulations of a single electron interacting resonantly with an EM wave in the presence of uniform static electric and magnetic fields, using classical equations of motion. These simulations elucidate the relationship between wave angular momentum and the resonance mechanism. Additionally, we compute the energy-transfer ratio from the electron's translational kinetic energy to its gyrokinetic energy during resonance, and the results show strong agreement with predictions from quantum theory.

The remainder of this paper is organized as follows. Section 2 develops the quantum theoretical framework incorporating angular-momentum conservation. Section 3 presents our numerical approach, detailing the simulation setup, analyzing the time evolution of electron velocity and kinetic energy, investigating the resonant conditions with wave angular momentum, and examining the energy-transfer ratio and polarization characteristics. Section 4 provides a comprehensive discussion of the key findings and their physical implications. Finally, Section 5 summarizes the principal conclusions and outlines potential directions for future research.

2. Quantum analysis of ADE

When a charged particle moves through a medium at a speed greater than the phase velocity of light in that medium, it induces polarization in the surrounding molecules. As these molecules return to their equilibrium state, they emit electromagnetic radiation. The constructive interference of these emissions produces the characteristic Cherenkov radiation, forming a cone-shaped wavefront, as shown in Fig. 1. The direction of Cherenkov radiation is constrained to the Cherenkov radiation angle $\theta_0 = \arccos(c'/v)$, where c' is the speed of light in the medium and v is the velocity of the charged particle.

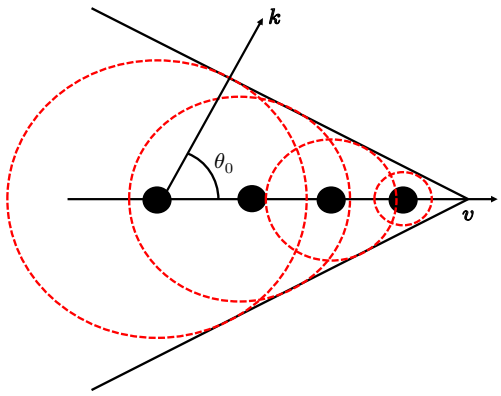


Fig. 1. Schematic diagram of Cherenkov radiation. The black points indicate snapshots of the electron at different times, the red dashed circle represents the current radiation surface from the previous electron.

However, when the electron is replaced by a system possessing internal energy — such as an oscillator or a cyclotron electron in a magnetic field — the direction of the emitted photon is no longer determined by the interference of secondary waves and can instead occur in any direction. Considering a scenario in which the system emits a photon with angular frequency ω and wavevector $\boldsymbol{k}$, the emission process must satisfy both energy and momentum conservation

$$T_1 + U_1 = \hbar\omega + T_2 + U_2, \tag{1a}$$

$$\boldsymbol{p}_1 = \boldsymbol{p}_2 + \hbar\boldsymbol{k}. \tag{1b}$$

Here, T and U represent the kinetic energy and internal energy of the system, while the subscripts 1 and 2 refer to the states before and after emitting a photon. $\boldsymbol{p}$ denotes the momentum of the system, and $\hbar$ represents the reduced Planck constant. Assuming that the photon's energy is far less than the initial kinetic energy T_1, the loss of kinetic energy after photon emission can be written as $\Delta T_{12} = T_1 - T_2 = \Delta\boldsymbol{p}\cdot\boldsymbol{v}$, where $\boldsymbol{v}$ is the velocity of the system before emission and $\Delta\boldsymbol{p} = \boldsymbol{p}_1 - \boldsymbol{p}_2 = \hbar\boldsymbol{k}$. Thus, the change in internal energy becomes

$$\Delta U_{21} = \Delta T_{12} - \hbar\omega = \hbar\boldsymbol{k}\cdot\boldsymbol{v} - \hbar\omega = \hbar\omega\left(\frac{v\cos\theta}{c'} - 1\right). \tag{2}$$

Here, $\omega/k = c'$, and $\Delta U_{21} = U_2 - U_1$. When the system's velocity exceeds the speed of light in the medium ($v > c'$), the sign of ΔU_{21} allows the radiation to be categorized into three distinct regions, as illustrated in Fig. 2.

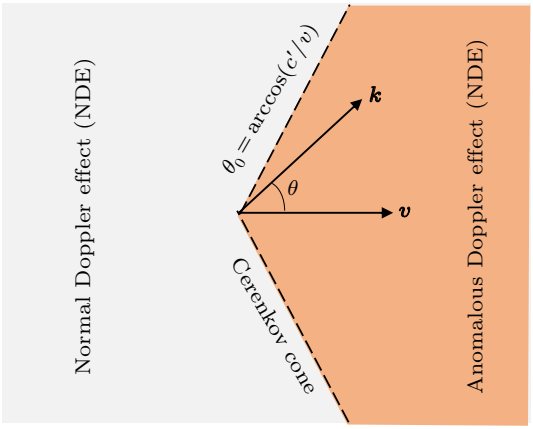


Fig. 2. Regions of the ADE and the NDE .

(i) For $\theta > \theta_0 = \arccos(c'/v)$, $\Delta U_{21} < 0$. The system produces photons by consuming both its internal and kinetic energy; this region corresponds to the normal Doppler effect (NDE).

(ii) For $\theta = \theta_0$, $\Delta U_{21} = 0$, and the loss of kinetic energy by the system is completely converted into photon energy; this line corresponds to the Cherenkov effect.

(iii) For $\theta < \theta_0$, $\Delta U_{21} > 0$. This region is referred to as the ADE, where the system gains internal energy after emitting photons. This means that the loss of kinetic energy is converted into both photon energy and internal energy.

In previous work, the change in internal energy was given as $\Delta U = m\hbar\omega_{ce}$, where $m = 0, \pm1, \pm2, \ldots$ represents the Landau level, as reported by Ginzburg,[24] Coppi,[22] Frolov,[25] Frank,[2] Tamm,[1] and Nezlin.[5] The above discussion revisits the foundational work of Ginzburg.[24] In the present paper, it is further demonstrated that m actually corresponds to the quantum number associated with the angular momentum of the emitted photon.

Let us consider the process in which an electron cyclotron system under a uniform magnetic field emits a photon along the z axis, as shown in Fig. 3. The moving electron has velocity v_z along the background magnetic field and cyclotron velocity $v_\perp$. The kinetic energy along z is $T = \gamma m_0 c^2 - m_0 c^2$, where γ denotes the Lorentz factor and m_0 refers to the electron's rest mass. The internal energy is approximated expressed as $U = \frac{1}{2}\gamma m_0 v_\perp^2$.

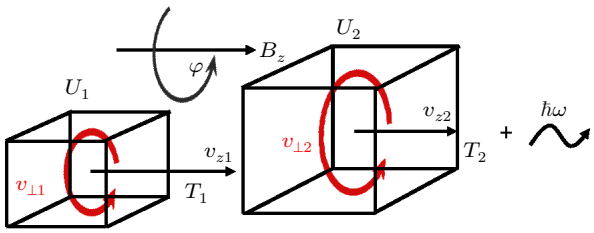


Fig. 3. Schematic diagram of the electron cyclotron system before and after photon emission. Here, $U_2 > U_1$ and $T_2 < T_1$.

Assume the angular momentum of the system before and after emitting a photon is L_1 and L_2, respectively. The angular momentum of the photon is $m\hbar$. According to angular-momentum conservation, we have

$$L_1 = L_2 + m\hbar. \tag{3}$$

Since the magnetic field is aligned along the z direction, the angular momentum of the electron along z is represented as L_z. According to quantum theory, the electron wave in a static magnetic field can be expressed as

$$\Psi = \Psi_0 \, \mathrm{e}^{\frac{\mathrm{i}}{\hbar}(\boldsymbol{p} - e\boldsymbol{A})\cdot\boldsymbol{s}}, \tag{4}$$

where Ψ_0 is the normalization coefficient, $\boldsymbol{A}$ is the vector potential, and $\boldsymbol{s}$ is the position. For a gyrating electron in a magnetic field, $\boldsymbol{s} = r\phi\,\boldsymbol{e}_\phi$, where r is the cyclotron radius and ϕ is the cyclotron angle.

The z-component of the orbital angular momentum operator can be expressed in spherical coordinates as

$$\hat{L}_z = -\mathrm{i}\hbar\frac{\partial}{\partial\phi}. \tag{5}$$

Combining Eq. (4) with Eq. (5), we have

$$-\mathrm{i}\hbar\frac{\partial}{\partial\phi}\Psi = (p_\phi - eA_\phi)\, r\Psi. \tag{6}$$

As a result, the eigenvalue of L_z can be expressed as

$$L_z = (p_\phi - eA_\phi)r. \tag{7}$$

With $p_\phi = \gamma m_0 v_\perp$, $A_\phi = \dfrac{rB_0}{2}$, and $r = \dfrac{\gamma m_0 v_\perp}{B_0 e}$, Eq. (7) can be rewritten as

$$L_z = \frac{1}{2}\cdot\frac{\gamma m_0 v_\perp^2}{\omega_{ce}} = \frac{U}{\omega_{ce}}, \tag{8}$$

where $\omega_{ce} = \dfrac{eB}{m_0\gamma} = \dfrac{\omega_0}{\gamma}$ and $U = \dfrac{1}{2}\gamma m_0 v_\perp^2$. Here, m_0 is the electron rest mass, γ is the Lorentz factor, and ω_0 is the electron cyclotron frequency in the rest frame (here we choose $\omega_0 > 0$). The conservation of angular momentum in the z-direction is expressed as

$$L_{z2} + m\hbar = L_{z1}.$$

The variation in the angular momentum of the electron along the z-axis is given by

$$\Delta L_{21} = L_{z2} - L_{z1} = \frac{U_2 - U_1}{\omega_{ce}} = -m\hbar. \tag{9}$$

Here, m is the quantum number of the photon's angular momentum in the z-direction. The internal-energy change is given by $\Delta U_{21} = U_2 - U_1$. With Eq. (9), it can be rewritten as

$$\Delta U_{21} = -m\hbar\omega_{ce}. \tag{10}$$

According to Eqs. (2) and (10), the change in electron energy can be written as

$$\hbar\boldsymbol{k}\cdot\boldsymbol{v} = \hbar\omega - m\hbar\omega_{ce}. \tag{11}$$

This result is consistent with previous findings.[1,2,5,22,25,26] Here, $\hbar\boldsymbol{k}\cdot\boldsymbol{v}$ represents the loss of kinetic energy ΔT_{12}, $\hbar\omega$ represents the photon energy, and $-m\hbar\omega_{ce}$ represents the change in electron gyrokinetic energy ΔU_{21}. The ratio between the internal-energy change ΔU_{21} and the kinetic-energy change ΔT_{21} is

$$\frac{\Delta U_{21}}{\Delta T_{21}} = \frac{m\hbar\omega_{ce}}{\hbar\boldsymbol{k}\cdot\boldsymbol{v}}. \tag{12}$$

This result is a critical criterion for comparison with the classical dynamic simulation in Section 2. It is also derived from classical theory in Appendix A. After simplifying Eq. (11), we finally obtain the classical wave–particle resonance condition

$$\omega = k_z v_z + m\omega_{ce}. \tag{13}$$

The variable m represents the quantum number associated with the angular momentum of the photon. Since a photon possesses both orbital angular momentum ($l\hbar$, where $l = 0, \pm1, \pm2, \ldots$) and intrinsic spin angular momentum ($s\hbar$, where $s = \pm1$),[27] the total angular momentum can be expressed as $m\hbar = l\hbar + s\hbar$.

For photons carrying only spin angular momentum, two distinct quantum states are possible, characterized by the spin quantum number m.

(i) For $m=+1$ ($\Delta U_{21}<0$), the cyclotron electron loses internal energy upon photon emission. The emitted photon exhibits right-hand circular polarization. This process is known as the NDE.

(ii) For $m=-1$ ($\Delta U_{21}>0$), the cyclotron electron gains internal energy through photon emission. The emitted photon exhibits left-hand circular polarization (the difference between our definition of circular polarization and the standard definition[28] stems from our choice of $\omega_0>0$. Here, $m>0$ corresponds to the same rotational sense as the electron's natural right-hand gyration, yielding right-hand polarization when $\boldsymbol{k}\parallel\boldsymbol{B}_0$). This process corresponds to the ADE.

The above discussion describes spontaneous emission phenomena of ADE and NDE without external-field intervention. In our simulation model, we introduce an external plane EM wave that serves as a resonant field interacting with electrons. This plane EM wave acts as an inducing field, enabling a gyro-electron to undergo stimulated absorption or emission processes. From a quantum perspective, the plane EM wave can be regarded as an ocean of photons that carry only spin angular momentum. Consequently, the same resonance conditions as those derived from quantum field theory are recovered.

(i) Right-hand circularly polarized waves correspond to $m=+1$ states,[29] resonating only when $\omega=\omega_{\rm ce}+\boldsymbol{k}\cdot\boldsymbol{v}$ (NDE condition).

(ii) Left-hand circularly polarized waves correspond to $m=-1$ states, resonating only when $\omega=-\omega_{\rm ce}+\boldsymbol{k}\cdot\boldsymbol{v}$ (ADE condition).

This exact correspondence between our classical simulation framework and quantum field-theoretic predictions validates our modeling approach while providing physical insight into the angular-momentum selection rules governing these resonant interactions.

Although nonlinear analyses of electron interactions with electromagnetic waves have been extensively studied,[30–38] the specific role of static electric fields in these interactions has received comparatively less attention. In our approach, the uniform electric field serves a crucial function by systematically scanning the electron velocity, thereby enabling investigation across the full spectrum of resonance conditions. The inherent complexity of these nonlinear processes precludes analytical solutions, necessitating the use of numerical simulation methods to obtain meaningful physical insights.

3. Classical dynamic simulation of ADR

The ADE process has been theoretically analyzed in the quantum framework, where the angular momentum carried by the emitted photon determines the resonance condition. To validate these characteristics in a classical picture, we investigate the interaction between an electromagnetic wave and an electron during ADR and NDR. The corresponding energy-transfer ratio can also be examined through numerical simulations.

3.1. Numerical simulation setup

To analyze the resonant process from the perspective of classical dynamics and to facilitate a direct comparison with the quantum results, we consider the following configuration. A uniform magnetic field $\boldsymbol{B}_0$ is applied along the z-direction. An electrostatic field $\boldsymbol{E}_0$, oriented opposite to $\boldsymbol{B}_0$ (as illustrated in Fig. 4), is introduced to accelerate the electron.

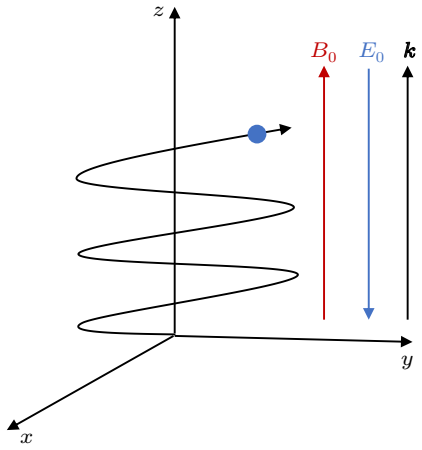


Fig. 4. Schematic of the setup: a uniform static magnetic field B_0 along the z-axis, an electrostatic field E_0 oriented opposite to B_0, and a wavevector $\boldsymbol{k}$ aligned parallel to B_0.

We consider the interaction between an electron entering the system with velocity v_z, parallel to the magnetic field $B_0=B_z$, and a linearly or circularly polarized transverse electromagnetic (TEM) wave propagating in a homogeneous dielectric medium with a refractive index $n>1$.

The induced linearly polarized wave along $\boldsymbol{B}_0$ can be decomposed into a combination of a right-hand circularly polarized wave ($m=1$) and a left-hand circularly polarized wave ($m=-1$), such that $\boldsymbol{E}_{\rm w}=\boldsymbol{E}_{\rm R}+\boldsymbol{E}_{\rm L}$, where $\boldsymbol{E}_{\rm R}=\frac{1}{2}E_0(\boldsymbol{e}_x+{\rm i}\boldsymbol{e}_y)\exp[{\rm i}(\boldsymbol{k}\cdot\boldsymbol{r}-\omega t)]$, $\boldsymbol{E}_{\rm L}=\frac{1}{2}E_0(\boldsymbol{e}_x-{\rm i}\boldsymbol{e}_y)\exp[{\rm i}(\boldsymbol{k}\cdot\boldsymbol{r}-\omega t)]$. The magnetic field of the EM wave is

$$\boldsymbol{B}_{\rm w}=\frac{\boldsymbol{k}\times\boldsymbol{E}_{\rm w}}{\omega}. \tag{14}$$

The six-dimensional phase space of an electron, described by its position $\boldsymbol{r}$ and momentum $\boldsymbol{p}$, is governed by the equations below. The vectors $\boldsymbol{E}$ and $\boldsymbol{B}$ represent the total field, including both static and electromagnetic components. Here, c denotes the speed of light in vacuum, e represents the electron's charge, and m_0 is the electron's rest mass

$$\frac{{\rm d}\boldsymbol{r}}{{\rm d}t}=\frac{\boldsymbol{p}}{\sqrt{m_0^2+\frac{\boldsymbol{p}^2}{c^2}}},$$

$$\frac{\mathrm{d}\boldsymbol{p}}{\mathrm{d}t} = -e\left(\boldsymbol{E}(\boldsymbol{r},t) + \frac{\boldsymbol{p}}{\sqrt{m_0^2 + \frac{p^2}{c^2}}} \times \boldsymbol{B}(\boldsymbol{r},t)\right). \quad (15)$$

To simulate the evolution of $\boldsymbol{r}$ and $\boldsymbol{p}$, the above system is discretized using the volume-preserving algorithm.[39,40] Let j denote the iteration step and $\mathrm{Cay}(\boldsymbol{A})$ represent the Cayley transform of matrix $\boldsymbol{A}$

$$\begin{cases} \boldsymbol{r}^*_{j+\frac{1}{2}} = \boldsymbol{r}^*_j + \frac{\Delta t^*}{2\gamma_j}\boldsymbol{p}^*_j, \\ \boldsymbol{p}^{*-} = \boldsymbol{p}^*_j + \frac{\Delta t^*}{2}\boldsymbol{E}^*_{j+\frac{1}{2}}, \\ \boldsymbol{p}^{*+} = \mathrm{Cay}\left(\frac{\Delta t^* \hat{\boldsymbol{B}}^*}{2\gamma^{*-}}\right)\boldsymbol{p}^{*-}, \\ \boldsymbol{p}^*_{j+1} = \boldsymbol{p}^{*+} + \frac{\Delta t^*}{2}\boldsymbol{E}^*_{j+\frac{1}{2}}, \\ \boldsymbol{r}^*_{j+1} = \boldsymbol{r}^*_{j+\frac{1}{2}} + \frac{\Delta t^*}{2\gamma_{j+1}}\boldsymbol{p}^*_{j+1}. \end{cases} \quad (16)$$

The dimensionless parameters are momentum $p^* = p/(m_0 c)$, magnetic field $B^* = B/(e\tau_{\mathrm{ce}} m_0)$, total electric field $E^* = E/[m_0 c/(\tau_{\mathrm{ce}} e)]$, time step $\Delta t^* = \Delta t/\tau_{\mathrm{ce}}$, and position $r^* = r/(\tau_{\mathrm{ce}} c)$, where τ_{ce} is the electron cyclotron period ($\tau_{\mathrm{ce}} = 2\pi/\omega_{\mathrm{ce}}$) and $\gamma^* = \sqrt{1+p^{*2}}$ is the Lorentz factor. The dimensionless magnetic matrix $\boldsymbol{B}^*$[39] is written as

$$\hat{B}^* = \begin{pmatrix} 0 & B^*_z & -B^*_y \\ -B^*_z & 0 & B^*_x \\ B^*_y & -B^*_x & 0 \end{pmatrix}. \quad (17)$$

To illustrate the system evolution, the parameters are set as follows: background magnetic field $B_0 = 0.02$ T, wave angular frequency $\omega_{\mathrm{s}} = 1.5\omega_0$ where $\omega_0 = eB_0/m_0$, wavevector $\boldsymbol{k} = 10^5$ m^{-1}, electric field component of the electromagnetic wave $E_{\mathrm{w}} = 9$ V/m. The induced wave propagates along the z axis with linear polarization, and the electrostatic field is $E_0 = -2.5$ V. The time step is chosen to satisfy $\Delta t = \min\left(\frac{2\pi}{50(\boldsymbol{k}\cdot\boldsymbol{v})}, \frac{2\pi}{50\omega_0}, \frac{2\pi}{50\omega_{\mathrm{s}}}\right)$ to ensure simulation accuracy.

The evolution of the electron's motion is shown in Fig. 5. As the electron accelerates from rest in the electrostatic field (Fig. 5(b)), the resonant frequencies increase simultaneously (Fig. 5(a)). The change in parallel velocity caused by the electromagnetic wave can be quantified as $\Delta v = v_z - v_{zE_0}$ (Fig. 5(c)), where v_z represents the parallel velocity under the combined fields, while v_{zE_0} denotes the parallel velocity resulting solely from the electrostatic field, which can be calculated as

$$v_{zE0} = \frac{eE_0 t}{m_0\sqrt{1+\left(\frac{eE_0 t}{m_0 c}\right)^2}}. \quad (18)$$

The cyclotron velocity is shown in Fig. 5(d). The work done by the electromagnetic wave is shown in Fig. 5(e), which can be calculated by integrating the power over time as $E_{\parallel\mathrm{emw}} = \int P_{\parallel\mathrm{emw}}\,\mathrm{d}t$, where $P_{\parallel\mathrm{emw}} = -e(\boldsymbol{v}_\perp \times \boldsymbol{B}_{\perp\mathrm{emw}})\cdot v_z$. Since all discrete data points are available from the simulation, numerical integration is straightforward. Figure 5(f) shows the gyrokinetic energy evolution over time, where $E_\perp = \frac{1}{2}m_0 v_\perp^2$.

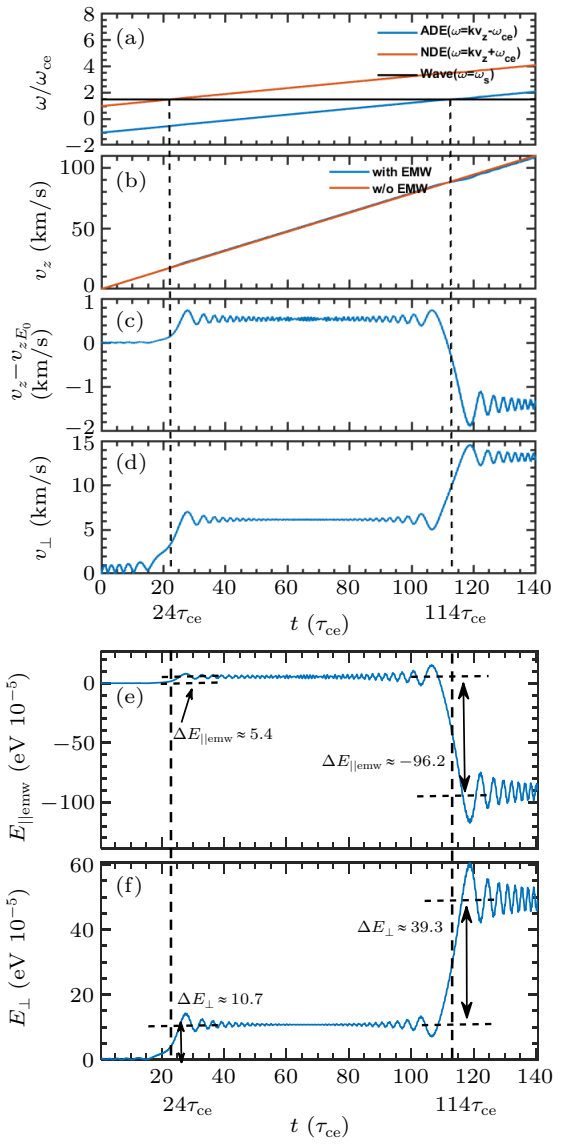


Fig. 5. Kinetic evolution of electrons in a magnetic field under the influence of an electromagnetic wave during acceleration. (a) Frequencies of ADE, NDE, and the source wave. (b) Parallel velocity v_z with and without the electromagnetic wave. (c) Change in parallel velocity induced by the electromagnetic wave. (d) Cyclotron velocity $v_\perp$. (e) Parallel kinetic energy transferred to the electron by the electromagnetic wave. (f) Evolution of gyro-kinetic (perpendicular) energy.

3.2. Validation of energy transfer ratio

As shown in Fig. 5(a), around $23\tau_{\mathrm{ce}}$, the normal Doppler frequency matches that of the induced wave, resulting in a rapid increase in the cyclotron velocity $v_\perp$ (Fig. 5(b)). Simultaneously, the change in parallel velocity induced by the electromagnetic wave also increases. This behavior can be interpreted as the electron cyclotron system absorbing a photon during the NDR, leading to an increase in both parallel kinetic energy and gyro-kinetic energy (internal energy).

The change in parallel kinetic energy due to the electromagnetic wave is shown in Fig. 5(e), where $\Delta T_{21} = \Delta E_{\parallel\mathrm{emw}} \approx 5.4 \times 10^{-5}$ eV. The corresponding increase in gyro-kinetic energy is $\Delta U_{21} = \Delta E_\perp \approx 10.7 \times 10^{-5}$ eV, also shown in Fig. 5(e). Consequently, the energy transfer ratio between

internal energy and parallel kinetic energy during resonance is $\frac{\Delta U_{21}}{\Delta T_{21}} \approx 1.98$. According to quantum theory (Eq. (12)), for $m = 1$ (NDE) and $k = 10^5$ m^{-1} along the z-axis, the resonant velocity is $v_z \approx 19 \times 10^3$ m/s and $\omega_{ce} \approx 3.51 \times 10^9$ s^{-1}. This yields $n_p = 1.85$, in close agreement with the simulation results.

The ADR begins to manifest at $t \approx 113\tau_{ce}$, where $\omega_{ADE} = \omega$ (Fig. 5(a)). At this point, the parallel velocity starts to scatter into the perpendicular direction, as evidenced by the decrease in Δv_z and the corresponding increase in $v_\perp$ (Figs. 5(c) and 5(d)). During the resonant period, the changes in parallel kinetic and gyro-kinetic energies due to the electromagnetic wave are $\Delta T_{21} = \Delta E_{\|emw} \approx -96.2 \times 10^{-5}$ eV, $\Delta U_{21} = \Delta E_\perp \approx 39.3 \times 10^{-5}$ eV. The resulting energy transfer ratio is $\frac{\Delta U_{21}}{\Delta T_{21}} \approx -0.408$. According to quantum theory, this ratio is given by $\frac{\Delta U_{21}}{\Delta T_{21}} = -\frac{\hbar\omega_{ce}}{\hbar \boldsymbol{k}\cdot\boldsymbol{v}} \approx -0.3908$, where $\omega_{ce} \approx 3.51 \times 10^9$ s^{-1}, $k = 10^5$ m^{-1}, and $v_z = 90$ km/s. The quantum theory prediction is in good agreement with the numerical results. The derivation of this energy change ratio based on classical theory is provided in Appendix A.

3.3. Validation of the relationship with wave angular momentum

Figures 6(a) and 6(b) show the velocity evolution under linear polarization E_l, right-circular polarization E_R ($m = -1$), and left-circular polarization E_L ($m = 1$). The work done on the electron by the electromagnetic wave, E_{emw}, depicted in Fig. 6(c), comprises the component along the parallel direction, $E_{\|emw}$, as previously described, and the work on gyro-kinetic energy, $E_{\perp emw}$. The latter is calculated as $E_{\perp emw} = \int \boldsymbol{F}_\perp \cdot \boldsymbol{v}_\perp \mathrm{d}t$, where $\boldsymbol{F}_\perp$ is determined from the electric and magnetic field forces, and $\boldsymbol{v}_\perp$ represents the cyclotron velocity. All these quantities can be obtained directly from the numerical results and integrated discretely. As shown in Fig. (6(c)), during the NDE period the electromagnetic wave performs positive work on the electron, an effect analogous to photon absorption. In contrast, during the ADE period the electromagnetic wave performs negative work, indicating that the electron emits photons in a manner similar to stimulated emission.

The three polarization types are investigated under the same scenario as before. As a result, the right-hand circularly polarized (RHCP) wave ($m = 1$) induces a velocity change only around $23\tau_{ce}$, whereas the left-hand circularly polarized (LHCP) wave ($m = -1$) induces a velocity change only around $113\tau_{ce}$. This confirms that the RHCP wave corresponds to the NDE, while the LHCP wave corresponds to the ADE, in agreement with the quantum analysis.

For a LHCP electromagnetic wave, the angular momentum selection rule ($m = -1$) restricts resonance to occur only when $\omega = \boldsymbol{k}\cdot\boldsymbol{v} - \omega_{ce}$, as confirmed numerically in Fig. 7. This represents a significant departure from previous classical treatments (Eqs. (36) and (37)),[23] which allowed resonance at arbitrary integer harmonics m, while remaining fully consistent with quantum angular momentum conservation principles.

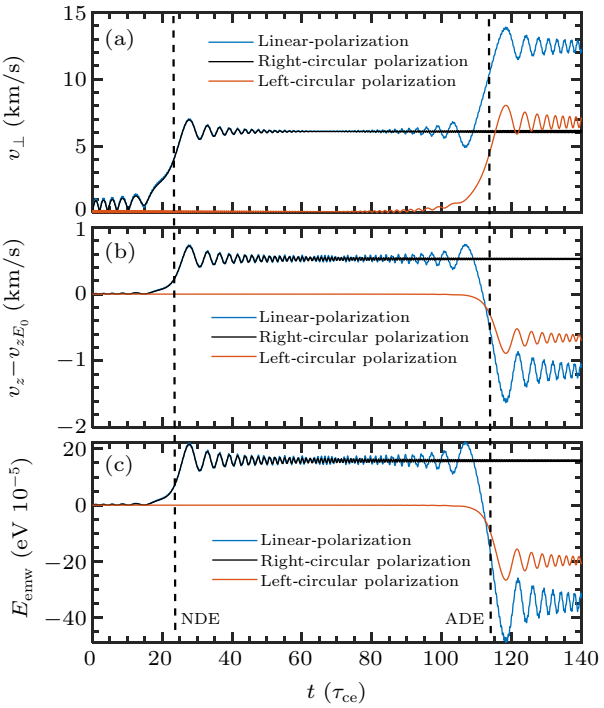


Fig. 6. Velocity evolution induced by waves with linear, right-circular, and left-circular polarization. (a) Cyclotron velocity $v_\perp$. (b) Change in parallel velocity caused by the electromagnetic wave.

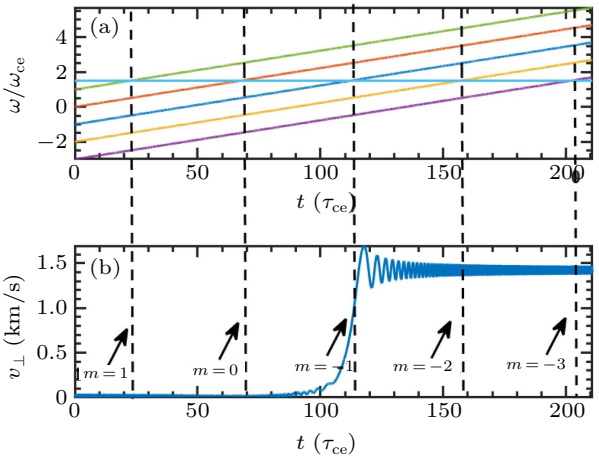


Fig. 7. (a) Frequency $\omega = \boldsymbol{k}\cdot\boldsymbol{v} + m\omega_{ce}$ for different m values and induced wave frequencies. (b) Evolution of perpendicular velocity under a left-circularly polarized wave ($m = -1$).

4. Discussion

Based on momentum and angular momentum conservation, let us consider the case where $\boldsymbol{k}$ is oriented opposite to $v_\|$ (or $\boldsymbol{B}_0$). In this scenario, if a cyclotron electron emits a photon with left-hand circular polarization and momentum $-\hbar\boldsymbol{k}$, carrying angular momentum $\hbar$, then after emission the change in internal energy is $\Delta U = -\hbar\omega_{ce} < 0$, while the change in translational kinetic energy is $\Delta T = \hbar k v_\| > 0$. In

contrast, if the emitted photon has right-hand circular polarization with momentum $-\hbar\boldsymbol{k}$, the change in internal energy becomes $\Delta U = \hbar\omega_{\rm ce} > 0$, while the translational kinetic energy remains $\Delta T = \hbar k v_\parallel > 0$. This scenario would violate energy conservation, since an electron cannot emit a photon while simultaneously increasing its total energy. Consequently, for a plane electromagnetic wave, only the left-circularly polarized component can resonate with an electron moving opposite to $v_\parallel$ (or $\boldsymbol{B}_0$).

The resonant condition can also be interpreted classically. In the case of ADR, where $\boldsymbol{k} \parallel \boldsymbol{v}$ and $v_z > c' \equiv \omega/|\boldsymbol{k}|$, the LHCP wave appears as a right-hand polarized wave in the cyclotron electron's rest frame, allowing resonance. In contrast, for normal Doppler resonance, where $v_z < c'$, the RHCP wave maintains its polarization in the electron's rest frame. However, when $\boldsymbol{k}$ is anti-parallel to $\boldsymbol{v}$ ($\boldsymbol{k}\cdot\boldsymbol{v} < 0$), only the LHCP wave preserves the same rotational direction as the electron's cyclotron motion, independent of the parallel velocity. Therefore, in this configuration, only left-hand polarized waves can resonate with the electron.

This study also provides a perspective on electron heating and current drive by EM waves. During the NDR process, the fraction of the electron's internal energy gain from the EM wave relative to the total absorbed wave energy can be expressed as $\eta_H = \frac{m\omega_{\rm ce}}{\omega}$, while the fraction contributing to parallel kinetic energy is $\eta_T = \frac{\boldsymbol{k}\cdot\boldsymbol{v}}{\omega}$. These relations can help optimize plasma heating and current drive efficiency. In the case of ADR, the electron's parallel kinetic energy can be converted into internal (gyro) energy, a mechanism that may contribute to suppressing runaway electron energies. This phenomenon has been studied previously,[9,20] but further investigation is warranted in future fusion tokamak plasmas.

5. Conclusion

This paper presents a simple yet effective approach for analyzing resonant processes associated with the NDE and ADE. By combining quantum theory with angular momentum conservation analysis, it is demonstrated that the parameter m in the resonance condition $\omega = \boldsymbol{k}\cdot\boldsymbol{v} + m\omega_{\rm ce}$ directly corresponds to the angular momentum of the resonant wave. Numerical simulations based on the volume-preserving algorithm (VPA) further support the quantum results, confirming both the angular momentum interpretation of m and the energy transfer characteristics. Future work will investigate the interaction between electron energy transformation and helicon waves in a plasma environment, aiming to provide deeper insights into applications such as plasma heating[41] and suppression of runaway electrons.

Appendix A: Classical analysis of anomalous Doppler resonance

Neglecting the static electric field and relativistic effects, we provide a brief derivation of the energy transformation process based on classical dynamical equations

$$m_{\rm e}\frac{{\rm d}\boldsymbol{v}_\parallel}{{\rm d}t} = -e(\boldsymbol{v}_\perp \times \boldsymbol{B}_\perp), \tag{A1}$$

$$m_{\rm e}\frac{{\rm d}\boldsymbol{v}_\perp}{{\rm d}t} = -e(\boldsymbol{v}_\perp \times \boldsymbol{B}_0 + \boldsymbol{v}_\parallel \times \boldsymbol{B}_\perp + \boldsymbol{v}_\perp \times \boldsymbol{B}_0). \tag{A2}$$

Consider $\boldsymbol{B}_\perp = \frac{\boldsymbol{e}_k \times \boldsymbol{E}_\perp}{v_p}$, where $\boldsymbol{e}_k$ is the unit vector along the wave vector of the electromagnetic wave, which is along the z-axis. Taking the dot product of $\boldsymbol{v}_\parallel$ and $\boldsymbol{v}_\perp$ with Eqs. (A1) and (A2), and substituting $\boldsymbol{B}_\perp$, we obtain

$$m_{\rm e}\boldsymbol{v}_\parallel \cdot \frac{{\rm d}\boldsymbol{v}_\parallel}{{\rm d}t} = -e(\boldsymbol{v}_\perp \cdot \boldsymbol{E}_\perp)\frac{v_\parallel}{v_p}, \tag{A3}$$

$$m_{\rm e}\boldsymbol{v}_\perp \cdot \frac{{\rm d}\boldsymbol{v}_\perp}{{\rm d}t} = e(\boldsymbol{v}_\perp \cdot \boldsymbol{E}_\perp)\frac{v_\parallel}{v_p} - e(\boldsymbol{v}_\perp \cdot \boldsymbol{E}_\perp). \tag{A4}$$

Here, $v_p = \omega/k$ is the phase velocity of the wave. Adding Eqs. (A3) and (A4) gives the total energy change of the electron

$$\frac{\rm d}{{\rm d}t}\left(\frac{1}{2}m_{\rm e}v_\parallel^2 + \frac{1}{2}m_{\rm e}v_\perp^2\right) = -e(\boldsymbol{v}_\perp \cdot \boldsymbol{E}_\perp). \tag{A5}$$

The sign of $-e(\boldsymbol{v}_\perp \cdot \boldsymbol{E}_\perp)$ determines whether the electromagnetic (E.M.) wave undergoes "emission" ($-e(\boldsymbol{v}_\perp \cdot \boldsymbol{E}_\perp) < 0$) or "absorption" ($-e(\boldsymbol{v}_\perp \cdot \boldsymbol{E}_\perp) > 0$), depending on the phase difference between $v_\perp$ and $E_\perp$.

From Eq. (A4) we have

$$e(\boldsymbol{v}_\perp \cdot \boldsymbol{E}_\perp) = \frac{m_{\rm e}\boldsymbol{v}_\perp \cdot \frac{{\rm d}\boldsymbol{v}_\perp}{{\rm d}t}}{\frac{v_\parallel}{v_p} - 1}. \tag{A6}$$

Substituting Eq. (A6) into Eq. (A3), we obtain

$$m_{\rm e}\boldsymbol{v}_\parallel \cdot \frac{{\rm d}\boldsymbol{v}_\parallel}{{\rm d}t} = -\frac{m_{\rm e}\boldsymbol{v}_\perp \cdot \frac{{\rm d}\boldsymbol{v}_\perp}{{\rm d}t}}{\frac{v_\parallel}{v_p} - 1}\frac{v_\parallel}{v_p}. \tag{A7}$$

Integrating Eq. (A7), we obtain the classical invariant of motion for the electron under ADR

$$\frac{1}{2}m_{\rm e}\left(v_\parallel - \frac{\omega}{k}\right)^2 + \frac{1}{2}m_{\rm e}v_\perp^2 = C_0, \tag{A8}$$

where C_0 is a constant determined by the initial conditions.

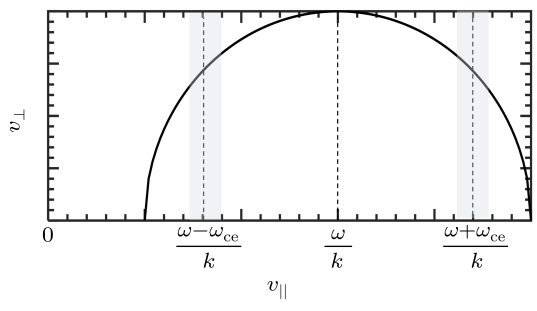


Fig. A1. Trajectory in the $(v_\parallel, v_\perp)$ plane.

Here, C_0 refers to the initial value. The change in velocity is constrained to a circular trajectory, as illustrated in Fig. A1. At the NDR, where

$$v_{\parallel} = \frac{\omega - \omega_{\rm ce}}{k},$$

an increase in $v_{\parallel}$ corresponds to an increase in $v_{\perp}$. In contrast, at the ADR, where

$$v_{\parallel} = \frac{\omega + \omega_{\rm ce}}{k},$$

an increase in $v_{\parallel}$ corresponds to a decrease in $v_{\perp}$.

The change of energy in translational energy and gyrokinetic energy can be written as

$$\frac{\Delta U}{\Delta T} = \frac{v_{\perp}\, dv_{\perp}}{v_{\parallel}\, dv_{\parallel}}. \tag{A9}$$

From Eq. (A8), we have

$$\frac{{\rm d}v_{\perp}}{{\rm d}v_{\parallel}} = -\frac{v_{\parallel} - \frac{\omega}{k}}{v_{\perp}}. \tag{A10}$$

Combining Eqs. (A9) and (A10), we obtain

$$\frac{\Delta U}{\Delta T} = -\frac{v_{\parallel} - \frac{\omega}{k}}{v_{\parallel}}. \tag{A11}$$

According to the resonant condition

$$\omega = k\, v_{\parallel} + m\, \omega_{\rm ce},$$

substituting $v_{\parallel}$ into Eq. (A11) yields

$$\frac{\Delta U}{\Delta T} = \frac{m\, \omega_{\rm ce}}{k v_{\parallel}}, \tag{A12}$$

which agrees with the quantum result in Eq. (12).

Acknowledgment

This project is supported by the National Magnetic Confinement Fusion Energy Program of China (Grant No. 2019YFE03020001).

References

[1] Tamm I E 1959 *Nobel Lectures* **18** 122
[2] Frank I M 1960 *Science* **131** 702
[3] Ginzburg V L 1960 *Sov. Phys. Usp.* **2** 874
[4] Shustin E G, Popovich P and Kharchenko I F 1971 *Sov. Phys. JETP* **59** 657
[5] Nezlin M V 1976 *Sov. Phys. Usp.* **19** 946
[6] Santini F, Barbato E and De Marco F 1984 *Phys. Rev. Lett.* **52** 1300
[7] Kho T H and Lin A T 1988 *Phys. Rev. A* **38** 2883
[8] Wang Y, Qin H and Liu J 2016 *Phys. Plasmas* **23** 062505
[9] Guo Z, McDevitt C J and Tang X Z 2018 *Phys. Plasmas* **25** 032504
[10] Liu C, Hirvijoki E and Fu G Y 2018 *Phys. Rev. Lett.* **120** 265001
[11] Shi X, Lin X and Kaminer I 2018 *Nat. Phys.* **14** 1001
[12] Filatov L V and Melnikov V F 2021 *Geomagn. Aeron.* **61** 1183
[13] Artsimovich L A, Bobrovskii G A and Mirnov S V 1967 *Sov. At. Energy* **22** 325
[14] Kadomtsev B B and Pogutse O P 1968 *Sov. Phys. JETP* **26** 1146
[15] Spong D A, Heidbrink W W and Paz-Soldan C 2018 *Phys. Rev. Lett.* **120** 155002
[16] Liu Y, Zhou T and Hu Y 2019 *Nucl. Fusion* **59** 106024
[17] Gorozhanin D V, Ivanov B I and Khoruzhiy V M 1997 *Waves excitation at anomalous Doppler effect for various electron beam energies,* Dec 31, 1997, Japan, pp. 402
[18] Sajjad S 2007 *Chin. Phys. Lett.* **24** 3195
[19] Castejon F and Eguilior S 2003 *Particle Dynamics under Quasi-linear Interaction with Electromagnetic Waves* (Madrid: Centro de Investigaciones Energeticas) p. 4
[20] Zhang Q, Zhang Y, Tang Q and Tang X Z 2024 arXiv:2409.15830 [physics.plasm-ph]
[21] Ginzburg N S 1979 *Radiophys. Quantum Electron.* **22** 323
[22] Coppi B, Pegoraro F, Pozzoli R and Rewoldt G 1976 *Nucl. Fusion* **16** 309
[23] Dendy R O 1987 *Phys. Fluids* **30** 2438
[24] Ginzburg V L 2005 *Acoust. Phys.* **51** 11
[25] Frolov V P and Ginzburg V L 1986 *Phys. Lett. A* **116** 423
[26] Ginzburg V L 1996 *Phys. Usp.* **39** 973
[27] Arnaut H H and Barbosa G A 2000 *Phys. Rev. Lett.* **85** 286
[28] Kiang D and Young K 2008 *Am. J. Phys.* **76** 1012
[29] Wei E, Lan Z, Chen M L, Chen Y P and Sun S 2024 *IEEE J. Multiscale Multiphys. Comput. Tech.* **9** 113
[30] Liu H, He X T, Chen S G and Zhang W Y 2004 arXiv:physics/0411183 [physics.plasm-ph]
[31] Qian B L 1999 *IEEE Trans. Plasma Sci.* **27** 1578
[32] Weyssow B 1990 *J. Plasma Phys.* **43** 119
[33] Gogoberidze G and Machabeli G Z 2005 *Mon. Not. R. Astron. Soc.* **364** 1363
[34] Roberts C S and Buchsbaum S J 1964 *Phys. Rev.* **135** A381
[35] Bourdier A and Gond S 2000 *Phys. Rev. E* **62** 4189
[36] Nusinovich G S, Korol M and Jerby E 1999 *Phys. Rev. E* **59** 2311
[37] Nusinovich G S, Latham P E and Dumbrajs O 1995 *Phys. Rev. E* **52** 998
[38] Qian B L 2000 *Phys. Plasmas* **7** 537
[39] Zhang R, Liu J, Qin H, Wang Y, He Y and Sun Y 2015 *Phys. Plasmas* **22** 044501
[40] Liu J, Wang Y and Qin H 2016 *Nucl. Fusion* **56** 064002
[41] Zhao Y, Bai J, Cao Y, Wu S, Ahedo E, Merino M and Tian B 2022 *Chin. Phys. B* **31** 075203